Molecular dynamics simulations of flavour molecules in Scotch whisky

Journal of Molecular Liquids 383 (2023) 122152

Contents lists available at ScienceDirect

Journal of Molecular Liquids

journal homepage: www.elsevier.com/locate/molliq

Molecular dynamics simulations of flavour molecules in Scotch whisky ☆

Emma E. Shuttleworth [a], Rui F.G. Apóstolo [a,*], Philip J. Camp [a], John M. Conner [b], Barry Harrison [b], Frances Jack [b], Joan Clark-Nicolas [b]

[a] School of Chemistry, University of Edinburgh, David Brewster Road, Edinburgh EH9 3FJ, Scotland, United Kingdom
[b] The Scotch Whisky Research Institute, Robertson Trust Building, Research Avenue North, Riccarton EH14 4AP, Scotland, United Kingdom

ARTICLE INFO

Keywords:
Scotch whisky
Molecular dynamics simulation
Liquid-vapour interface

ABSTRACT

Molecular dynamics simulations are used to investigate the interfacial properties of molecules related to flavours of Scotch whisky, in ethanol/water solutions with different values of alcohol-by-volume (ABV). The propensity of flavour molecules to accumulate at the liquid-vapour interface is linked to the evaporation of those molecules into the head space, and consequently their perception when nosing or tasting. The simulation approach is first validated for ethanol/water solutions, without flavour molecules, by comparing simulated and experimental values of the ethanol surface excess and the interfacial tension. The chosen values of ABV are 0% (pure water), 20% (typical dilution for sensory evaluation), 30% (diluted spirit), 40% (typical bottle strength), 50%, 65% and 73% (representing a range of cask strengths), and 100% (pure ethanol). Then, flavour molecules are considered, ranging from hydrophobic to hydrophilic: octane (alkane); octan-1-ol (alcohol); octanal (aldehyde); octanoic acid (carboxylic acid); and ethyl hexanoate (ester). The primary focus is whether there is a positive excess of such molecules at the interface, or whether the molecules remain fully solvated by the liquid layer. The dependence of this excess on ethanol content can be correlated with how flavour molecules are released into the head space on dilution with water, and hence the tasting experience. Additional molecular-level details are presented, such as how organic molecules are oriented with respect to the interface. This illustrates how molecular simulations could be employed to improve our understanding of the links between composition and flavour perception, or to aid the development of low-alcohol spirits with similar sensory characteristics to full strength equivalents.

1. Introduction

Although distilled spirits are mostly composed of ethanol and water, their distinct flavours and aromas arise from a plethora of small molecules which are present at significantly lower concentrations [1]. Scotch whisky contains a wide variety of naturally occurring flavour compounds which originate from the raw materials, production and maturation processes. The concentration, or even presence, of those molecules in whisky depends on a number of factors such as the malting procedure [2], the nature of the microorganisms present during the fermentation [3,4], and the treatment given to the oak casks in which the spirit is matured [5]. This results in significantly different flavour profiles across different Scotch whisky brands. In addition to the developing flavour composition, the alcoholic strength of the spirit also changes during production. According to legislation set out in the Scotch Whisky Regulations 2009 [6], the alcoholic strength of newly distilled spirit must be less than 94.8% alcohol by volume (ABV). Grain whiskies are generally distilled to strengths higher than 90% ABV, while for a typical malt whisky the distillation strength is around 68–70% ABV. The evaporation of alcohol (including the “angel’s share”), the addition of water, and the concomitant reduction in alcoholic strength continue from the time the spirit leaves the still until it reaches the glass. There is generally a dilution step before maturation, as water is an essential factor in the extraction of flavour from the oak. There is further dilution before bottling. By its legal definition, Scotch whisky needs to be bottled at a minimum alcohol strength of 40% ABV [6], but most is bottled at 40–43% ABV, although bottlings of higher strength can be found on the market. Finally, the consumer may choose to dilute their whisky further, depending on personal taste, by adding water or ice.

☆ Myroslav Holovko Virtual Special Issue.

* Corresponding author.
E-mail addresses: emmashuttle@btinternet.com (E.E. Shuttleworth), rui.apostolo@ed.ac.uk (R.F.G. Apóstolo), philip.camp@ed.ac.uk (P.J. Camp), jmc@swri.co.uk (J.M. Conner), barry.harrison@swri.co.uk (B. Harrison), fj@swri.co.uk (F. Jack), joan.clark88@gmail.com (J. Clark-Nicolas).

https://doi.org/10.1016/j.molliq.2023.122152
Received 6 March 2023; Received in revised form 12 May 2023; Accepted 17 May 2023
Available online 22 May 2023

The whisky industry uses sensory analysis – the evaluation by trained human assessors – to monitor and control flavour quality. Typically, assessments are carried out at 20% ABV. This reduces the burning sensation caused by alcohol, which interferes with the perception of other flavours and results in sensory fatigue [7]. Relatively little is understood about how differences in alcoholic strength affect the flavour of whisky. This question is commonly addressed by using chromatographic methods to study the distribution of molecules between the liquid and the head space (the vapour region in the glass, in immediate contact with the liquid). In some cases, the concentration of a target flavour molecule in the liquid phase falls below the limit of detection of traditional analytical methods, while still being detected in sensory analysis. This renders common experimental methods useless. In this work, the issue is addressed by using molecular simulations of flavour molecules at the liquid-vapour interface.

Molecular simulations have been widely used to study the microscopic behaviour of physicochemical systems in situations where experiments are difficult or impossible. Of particular importance to the current problem are binding and adsorption. In the pharmaceutical industry, virtual screening can be used to predict the binding affinity of millions of different small molecules to a macromolecule of therapeutic interest [8–10]. Molecular simulations are widely used to explore the adsorption of surfactant molecules at solid-liquid and liquid-vapour interfaces [11,12]. Molecular simulations have also been successfully applied to important problems in the drinks industry. In two recent studies by Du et al., the stability of Barley Limit Dextrinase (an enzyme that breaks barley starch into fermentable sugars) at different mashing temperatures was examined using molecular dynamics (MD) simulations [13,14]. A key publication on whisky by Karlsson and Friedman reports the interfacial properties of guaiacol (a phenol associated with smoky aroma in whisky) at different alcohol concentrations, and links these to the tasting experience [15]. MD simulations of a layer of ethanol/water solution were carried out, and the distribution of the solute (guaiacol) within the layer was computed, and linked to its likely evaporation, and hence sensing, in the head space.

Inspired by the work of Karlsson and Friedman [15], the current study is focused on a comparison of model flavour molecules with different functional groups, in solutions with different alcoholic strengths. The differences in the flavour of whisky at different alcohol strengths are due to different distributions of flavour molecules between the liquid (which is mostly ethanol and water) and the gas phase. Fig. 1 illustrates that a typical whisky drink can be simulated as an ethanol/water solution with or without flavour molecules (depending on the purpose), and with at least one liquid-air interface. The flavour molecules evaporate and resolvate at different rates depending on their physicochemical properties.

To validate the simulation approach, ethanol solutions of various concentrations are first studied without flavour molecules. Estimates of the surface excess of ethanol at the liquid-vapour interface, and the interfacial tension, are compared to experimental data from the literature. Because the solution layers are quite thin, the surface excess represents a significant fraction of the total ethanol content, and so an effective ABV of the bulk solution is derived in order to connect the simulated solutions with real spirits. Next, flavour molecules are added to the solution layers, and the spatial distributions of those molecules within the layers are computed, and subsequently linked to sensory perceptions. The flavour molecules are all linear, 8-carbon organic molecules related to typical whisky flavours, and include an alkane, an alcohol, an aldehyde, a carboxylic acid, and an ester. The findings contribute to the development of a better understanding of how alcoholic strength affects the solvation and evaporation of molecules related to the flavour of whisky and, in turn, the tasting experience.

The rest of this article is organised as follows. The MD simulation methods are described in Section 2. The results are presented in Section 3, beginning with ethanol solutions without flavour molecules (3.1), and then moving through each kind of flavour molecule (3.2).

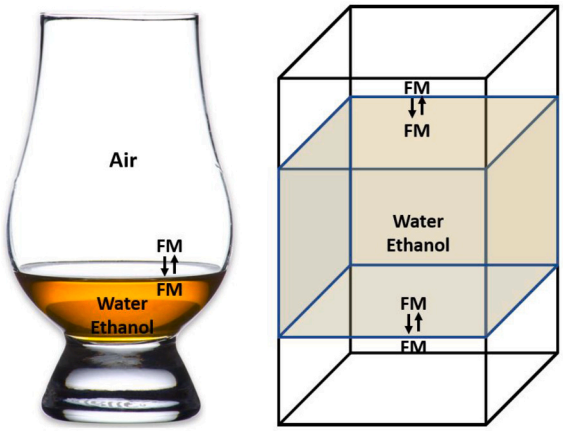

Fig. 1. Image of a typical whisky glass beside a schematic view of the MD simulation box used in this study. The spirit is approximated as an ethanol/water solution in which flavour molecules (FM) evaporate and resolvate at the edge of the liquid phase (brown).

The link between simulation results and flavour characteristics is outlined in Section 4, and Section 5 concludes the article.

2. Methods

The target molecules, listed in Table 1, were chosen to represent a wide range of flavours, and have different degrees of polarity. Descriptions of the flavours, and whether these are perceived as aromas or taste, are given in the table. An aroma compound can be perceived by the orthonasal route, breathed in through the nose and detected by the olfactory epithelium at the top of the nasal cavity, or retronasally, when the product is tasted and the compounds travel from the oral cavity up through the back of the nose to be detected by the same organ. Certain compounds, in this case octanoic acid, will generate a taste response, through stimulation of the taste buds on the tongue. Although octane does not represent a flavour, it was included due to its high hydrophobicity, and again 8-carbon structure. In order to understand the behaviour of the molecules in Table 1 at different alcoholic strengths, MD simulations were run under different conditions in which whisky can be consumed, in order of increasing ABV: sensory analysis (20%); diluted spirit (30%); bottle strength (40%); and cask strength (50%, 65%, 73%). Additionally, simulations with the same flavour compounds were run using pure water (0% ABV) and pure ethanol (100% ABV) as solvent. The analysis included the determination of concentration profiles across the liquid and head-space phases in order to provide insight on the effects that different alcohol concentrations can have on the evaporation of flavour molecules.

2.1. Molecular dynamics simulations

Classical MD simulations were performed using the LAMMPS software package [16–18] with initial configurations created using Packmol [19]. The Visual Molecular Dynamics software was used for system visualisation and image rendering [20]. The interactions between the target flavour molecules and ethanol were given by the all-atom L-OPLS-AA force field [21–25], while water interactions were given by the TIP3P force field [26]. Cross interactions were evaluated using the Good-Hope and Berthelot rules for the Lennard-Jones energy parameter and range parameter, respectively [27,28]. Liquid-vacuum interface simulations (modelling the liquid-vapour interface) were carried out on a square prism simulation box with periodic boundary conditions applied, Lennard-Jones interactions cut at 12 Å, and long-range Coulomb interactions handled using the particle-particle particle-mesh method with a relative accuracy in the forces of 1×10^{-4}. The dimensions of the box were $L_x = L_y = 80$ Å, and $L_z = 240$ Å.

Table 1
The target molecules studied in this work along with their chemical formulas, associated flavours, and whether they are aroma or taste compounds.

molecule	formula	flavour
octane	$CH_3(CH_2)_6CH_3$	none
octan-1-ol	$CH_3(CH_2)_6CH_2OH$	waxy (aroma)
octanal	$CH_3(CH_2)_6CHO$	soapy, oily (aroma)
octanoic acid	$CH_3(CH_2)_6COOH$	goaty (aroma), sour (taste)
ethyl hexanoate	$CH_3(CH_2)_4COOCH_2CH_3$	fruity (aroma)

Table 2
Details of the numbers of water and ethanol molecules used in the MD simulations. Component 1 is water, and component 2 is ethanol. N_i and x_i are, respectively, the number and mole fraction of component i, and $N_{\rm atom}$ is the total atom count. V_i is the molar volume of pure component i, $V_{\rm ex}$ is the excess molar volume calculated using Eq. (1), $V = x_1V_1 + x_2V_2 + V_{\rm ex}$ is the molar volume of the resulting solution, and the nominal ABV $= 100x_2V_2/V$.

N_1	N_2	$N_{\rm atom}$	x_1	x_2	x_1V_1 ($\rm cm^3\,mol^{-1}$)	x_2V_2 ($\rm cm^3\,mol^{-1}$)	$V_{\rm ex}$ ($\rm cm^3\,mol^{-1}$)	V ($\rm cm^3\,mol^{-1}$)	nominal ABV (%)
8500	0	25500	1.0000	0.0000	18.0687	0.0000	0.0000	18.0687	0.0000
6928	524	25500	0.9297	0.0703	16.7982	4.1266	−0.3583	20.5665	20.0646
6194	786	25656	0.8874	0.1126	16.0340	6.6084	−0.5573	22.0852	29.9224
5364	1048	25524	0.8366	0.1634	15.1155	9.5918	−0.7570	23.9503	40.0488
4510	1332	25518	0.7721	0.2279	13.9504	13.3759	−0.9366	26.3897	50.6861
3252	1700	25056	0.6567	0.3433	11.8658	20.1465	−1.0716	30.9407	65.1133
2585	1913	24972	0.5747	0.4253	10.3845	24.9577	−1.0703	34.2719	72.8228
0	2616	23544	0.0000	1.0000	0.0000	58.6857	0.0000	58.6857	100.0000

A cubic layer of solution containing water, ethanol, and flavour molecules with random positions and orientations was placed in the centre of the box. The numbers of water and ethanol molecules were chosen to give a desired nominal ABV (the volume of *pure* alcohol in a given volume of *solution*), while giving a similar total volume of liquid in each case. This involved correcting for the excess volume $V_{\rm ex}$ using the experimental data reported in [29], which were refitted using the equation

$$V_{\rm ex} = x_1(1-x_1)\sum_{n=0}^{4} A_n\,(2x_1-1)^n \tag{1}$$

where x_1 is the mole fraction of water. The refitted coefficients, all to 4 significant figures and in units of $\rm cm^3\,mol^{-1}$, are $A_0 = -4.140 \pm 0.040$, $A_1 = -1.200 \pm 0.149$, $A_2 = -2.746 \pm 0.355$, $A_3 = 0.1342 \pm 0.3162$, and $A_4 = 2.995 \pm 0.569$, and are not significantly different from those reported (without fitting errors) in [29]. The resulting numbers of molecules used in the simulations are summarised in Table 2, corresponding to nominal ABV values of approximately 0%, 20%, 30%, 40%, 50%, 65%, 73%, and 100%. In all cases, the systems were energy minimised, and then run at constant volume and temperature (NVT conditions) with $T = 298.15$ K using a Nosé-Hoover thermostat. The simulation time step was 1 fs, and typical run lengths, after equilibration, were 5 ns, over which various properties were computed and averaged.

2.2. Analysis

At equilibrium, the two liquid-vapour interfaces associated with the layer of solution are aligned, on average, in the xy plane, and the concentrations of the various components depend only on z. The total atom count was chosen so that the thickness of the resulting liquid layer was around 40 Å, which was large enough for the two interfaces to be independent of one another. In each case, the number of flavour molecules was 20, which was low enough for the concentration to be representative of real whisky, while improving statistics on the distribution throughout the liquid layer.

In what follows, the position $z = 0$ corresponds to the centre of mass of the liquid layer, and so $-L_z/2 \le z \le L_z/2$. Concentration profiles were analysed in two ways: using the local mass density of atoms belonging to a particular type of molecule, calculated within slices of width $\delta z = 0.1$ Å; and for the flavour molecules, which are at low concentration, the probability density $p(z)$ of finding particular groups of atoms within the liquid layer, defined so that $\int_{-L_z/2}^{L_z/2} p(z)dz = 1$.

The interfacial tension γ was calculated from the pressure tensor $P_{\alpha\beta}$ obtained from simulations. The relationship between these properties is [30]

$$\gamma = \int_{-\infty}^{+\infty} \left[P_{\rm N}(z) - P_{\rm T}(z)\right] dz, \tag{2}$$

where $P_{\rm N}$ is the normal component ($P_{\rm N} = P_{zz}$), and $P_{\rm T}$ is the transverse component [$P_{\rm T} = \left(P_{xx} + P_{yy}\right)/2$], with respect to an interface. Recall that the interfaces are parallel to the xy plane, and z is perpendicular to the interfaces, and so the pressure tensor (on average) depends on z only. The average of the pressure tensor over the simulation cell is therefore

$$\overline{P}_{\alpha\beta} = \frac{1}{L_z}\int_{-L_z/2}^{L_z/2} P_{\alpha\beta}(z)dz \tag{3}$$

and this is computed straightforwardly in LAMMPS. Note that in a liquid, the off-diagonal elements of the pressure tensor ($\alpha \neq \beta$) average out to zero, because liquids do not support shear stress. Inserting Eq. (3) into Eq. (2) gives the result

$$\gamma = \frac{L_z}{2}\left[\overline{P}_{zz} - \frac{\left(\overline{P}_{xx} + \overline{P}_{yy}\right)}{2}\right], \tag{4}$$

where the division by 2 is because there are two interfaces associated with the layer of liquid. γ was determined from Eq. (4) over the course of the MD simulation, and averaged.

3. Results

To set the scene, Fig. 2 shows final configurations of two ethanol solutions at 73% ABV with (a) octane and (b) octanoic acid. It is clear from the image that the octane molecules accumulate at the liquid-vapour interface, while there is some ingress of octanoic acid into the middle of the liquid layer. This simply reflects the relative polarity – and hydrophobicity – of each solute. The corresponding concentration profiles are examined in more detail in Section 3.2.

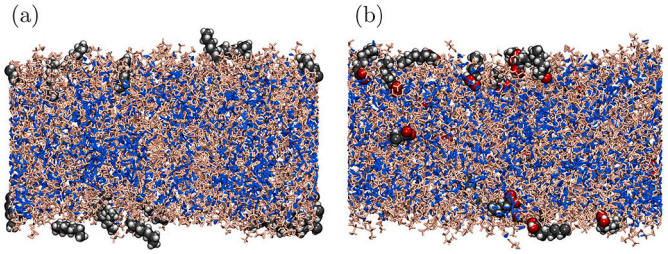

Fig. 2. Snapshots of 73% ABV solutions of (a) octane and (b) octanoic acid. Flavour molecules are shown in space filling representation: carbon – black; hydrogen – white; oxygen – red. Solvent molecules are shown in stick representation: water – blue; ethanol – orange.

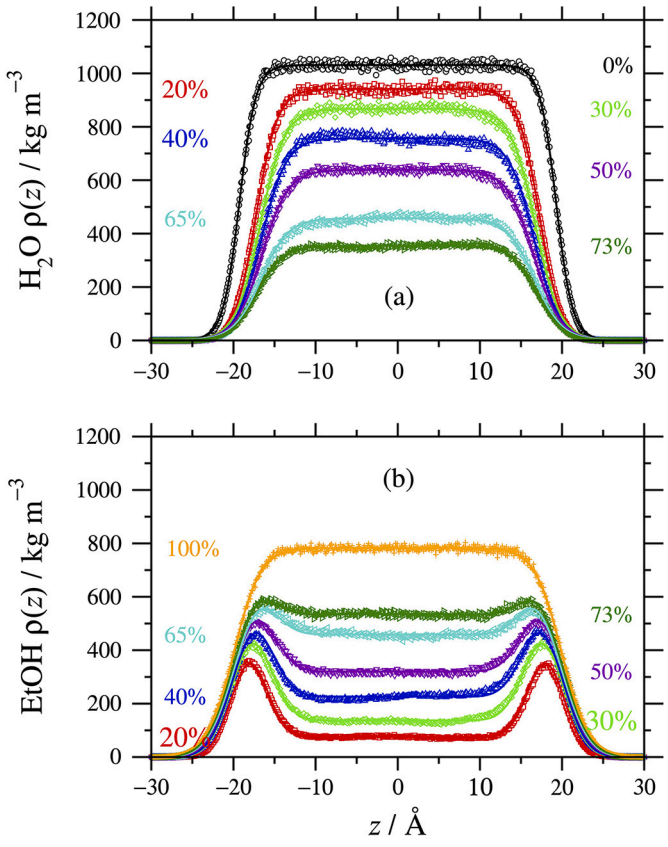

Fig. 3. Mass-density profiles of (a) water and (b) ethanol in liquid layers with different values of nominal ABV. The points are from MD simulations: 0% – black circles; 20% – red squares; 30% – light green diamonds; 40% – dark blue up triangles; 50% – purple down triangles; 65% – light blue left triangles; 73% – dark green right triangles; 100% – gold pluses. The lines are fits using Eq. (6): for the water profiles at all ABVs, and the pure-ethanol profile, there are no peaks at the liquid-vapour interfaces, and so $\Delta\rho = 0$. The fit parameters are given in Table 3.

3.1. Ethanol/water solutions

Fig. 3 shows the water and ethanol mass-density profiles in liquid layers with various values of ABV. In the pure-water case, the mass density in the middle of the layer is just 3% higher than the expected value for the bulk liquid at 25 °C ($\rho = 1031$ kg m^{-3} versus 997 kg m^{-3} [31]). As the ethanol content is increased, the shoulders of the water profile become broader, signalling that ethanol is competing with water at the interfaces.

To quantify these effects, the water-density profiles were fitted with the mean-field function [30]

$$\rho(z) = \frac{1}{2}\left(\rho_{\rm liq} + \rho_{\rm vap}\right) - \frac{1}{2}\left(\rho_{\rm liq} - \rho_{\rm vap}\right)\tanh\left(\frac{|z| - H/2}{\xi}\right), \tag{5}$$

where $\rho_{\rm vap}$ and $\rho_{\rm liq}$ are, respectively, the mass densities in the centres of the vapour and the liquid phases, H is the layer thickness, the interfaces are located at $z = \pm H/2$, and ξ is a measure of the interfacial thickness. For all practical purposes, $\rho_{\rm vap} = 0$. The fits are shown in Fig. 3(a), and the fit parameters are given in Table 3. As the ethanol content is increased, the width of the corresponding interface increases. Since H depends on the total atom count, it does not indicate anything of experimental relevance. The functional form of $\rho(z)$ depends on various theoretical approximations. For example, capillary wave theory gives an error function instead of a tanh function [32], but the quality of the fits, and the trends in $\rho_{\rm liq}$ and ξ, are practically the same.

The ethanol profiles can be fitted with the same function as Eq. (5), supplemented by Gaussian peaks centred at $z = \pm H/2$, and again with $\rho_{\rm vap} = 0$:

$$\rho(z) = \frac{1}{2}\rho_{\rm liq}\left[1 - \tanh\left(\frac{|z| - H/2}{\xi}\right)\right] + \Delta\rho\exp\left[-\frac{(|z| - H/2)^2}{2\sigma^2}\right]. \tag{6}$$

The fit parameters are given in Table 3. As the ethanol content is increased to 65%, the width of the interface increases slightly, and there are two clear peaks at the liquid-vapour interface, showing that there is a positive surface excess. In 100% ethanol, the liquid density is about 1% lower than the experimental value (785.2 kg m^{-3} [33]), and there is no surface excess. An estimate of the surface excess can be obtained from the area of each Gaussian peak in Eq. (6):

$$\Gamma_2^{\rm ex} = \frac{1}{2m_2}\int_{-\infty}^{\infty}\Delta\rho\exp\left[-\frac{(|z| - H/2)^2}{2\sigma^2}\right]dz = \frac{\sqrt{2\pi}\Delta\rho\,\sigma}{m_2}. \tag{7}$$

The peaks at $z = \pm H/2$ are assumed to be well separated, and m_2 is the molar mass of ethanol. Since thin liquid layers are used in the MD simulations, the surface excess of ethanol at the interface is significant compared to the amount of ethanol in the bulk solution. Therefore, the effective bulk mole fraction of ethanol is computed from

$$x_2^{\rm eff} = \frac{\rho_{\rm liq,2}/m_2}{\rho_{\rm liq,1}/m_1 + \rho_{\rm liq,2}/m_2} \tag{8}$$

where $\rho_{\rm liq,1}$ and $\rho_{\rm liq,2}$ refer to water and ethanol, respectively, and m_1 is the molar mass of water. Fig. 4 shows (a) the ethanol surface excess ($\Gamma_2^{\rm ex}$), and (b) the interfacial tension (γ), as functions of the (effective) mole fraction of ethanol in solution. The MD simulation results are compared with experimental data for both $\Gamma_2^{\rm ex}$ [34,35] and γ [36–38]. In general, the MD simulation results indicate a smaller surface excess and interfacial tension than seen experimentally, highlighting the shortcomings of the force field, and particularly TIP3P water [39]. But the position of the maximum in $\Gamma_2^{\rm ex}$, and the general composition dependence of γ, are both captured correctly by the simulations. Surface properties are particularly sensitive to the details of the interactions, and so it is encouraging that the MD simulation results are qualitatively correct.

As an aside, the TIP3P water model was chosen not for its accuracy in predicting bulk and interfacial properties – which is rather low [26,39–43] – but for its simplicity, and continued and widespread use in the molecular-simulation community, especially in conjunction with the OPLS-AA force field. Mixing force fields for different components rapidly increases the number of possible combinations. Gereben and Pusztai compared different water models in combination with OPLS-AA ethanol, and found that either the SWM4-DP or TIP4P-2005 model performs well compared to experimental data depending on the composition [44]. So the choice of force fields is complicated for mixtures. For completeness, some radial distribution functions (RDFs) for the current model are presented in Fig. 5. Bulk-phase *NPT* simulations were carried out in a cubic simulation box with $P = 1$ atm and $T = 298.15$ K, using the Nosé-Hoover barostat and thermostat.

Table 3
Parameters from the fits of Eqs. (5) and (6) to the density profiles of the ethanol/water solutions, and results from Eqs. (7) and (8). ρ_{liq} is the mass density in the centre of the liquid phase, H is the layer thickness, ξ is a measure of the interfacial thickness, x_2^{eff} is the effective bulk mole fraction of ethanol, and Γ_2^{ex} is the ethanol surface excess. Both the nominal and effective ABVs are given.

nominal ABV (%)	species	ρ_{liq} (kg m^{-3})	H (Å)	ξ (Å)	$\Delta\rho$ (kg m^{-3})	σ (Å)	x_2^{eff}	effective ABV (%)	Γ_2^{ex} (μmol m^{-2})
0	H_2O	1031.2 ± 0.5	38.56 ± 0.01	2.00 ± 0.01					
20	H_2O	941.2 ± 0.6	34.47 ± 0.01	2.60 ± 0.01					
20	EtOH	75.6 ± 0.3	36.39 ± 0.12	2.64 ± 0.74	310.4 ± 1.0	2.26 ± 0.01	0.0305	9.7	3.816 ± 0.015
30	H_2O	867.1 ± 0.6	33.49 ± 0.02	3.00 ± 0.01					
30	EtOH	137.3 ± 0.5	36.00 ± 0.17	2.90 ± 0.66	349.6 ± 2.0	2.55 ± 0.01	0.0583	17.5	4.843 ± 0.032
40	H_2O	757.0 ± 0.7	33.20 ± 0.02	3.03 ± 0.02					
40	EtOH	226.5 ± 0.6	35.98 ± 0.22	2.99 ± 0.51	337.0 ± 4.1	2.60 ± 0.01	0.1047	28.9	4.762 ± 0.061
50	H_2O	638.7 ± 0.5	33.11 ± 0.02	3.20 ± 0.02					
50	EtOH	320.4 ± 0.5	36.18 ± 0.19	3.12 ± 0.29	320.9 ± 4.6	2.70 ± 0.01	0.1640	40.9	4.714 ± 0.069
65	H_2O	457.2 ± 0.6	33.35 ± 0.03	3.31 ± 0.02					
65	EtOH	459.4 ± 0.6	36.49 ± 0.26	3.18 ± 0.22	254.4 ± 8.8	2.80 ± 0.02	0.2821	58.7	3.875 ± 0.137
73	H_2O	354.3 ± 0.4	34.16 ± 0.02	3.11 ± 0.02					
73	EtOH	535.6 ± 0.5	37.09 ± 0.25	3.26 ± 0.16	217.7 ± 9.9	2.76 ± 0.02	0.3715	68.4	3.267 ± 0.149
100	EtOH	782.8 ± 0.5	39.94 ± 0.07	3.23 ± 0.01				100.0	

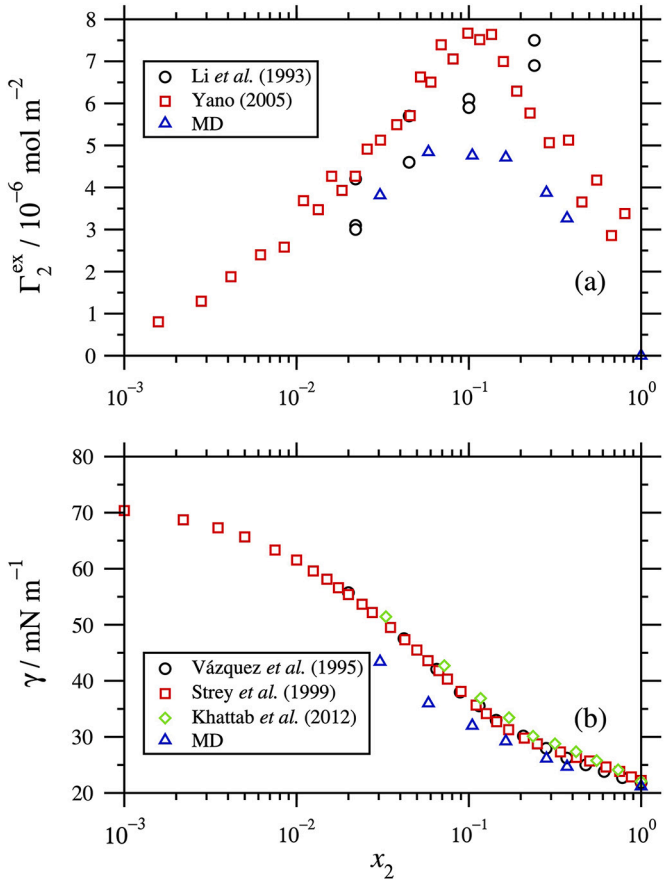

Fig. 4. (a) Ethanol surface excess Γ_2^{ex} and (b) interfacial tension γ as functions of the ethanol mole fraction x_2 from experiments and MD simulations. In the case of MD simulations, the effective ethanol mole fraction x_2^{eff} is used in place of x_2. For Γ_2^{ex}, experimental results are shown from Li et al. [34], and Yano [35]. For γ, experimental results are shown from Vázquez et al. [36], Strey et al. [37], and Khattab et al. [38].

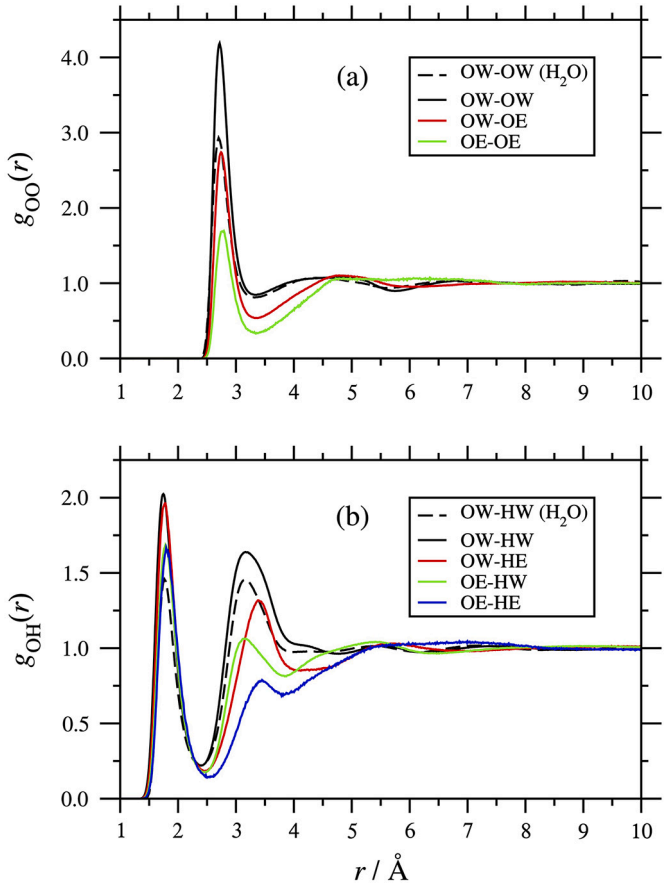

Fig. 5. Radial distribution functions $g(r)$ between (a) oxygen atoms of water (OW) and ethanol (OE), and (b) oxygens (OW, OE) and hydroxyl hydrogens (HW, HE). Results are shown for bulk simulations of pure water (black dashed lines) and 40% ABV solutions (solid lines).

Fig. 5(a) shows the oxygen-oxygen RDFs [$g_{OO}(r)$] in pure water, and in 40% ABV ethanol solution ($x_2 = 0.1634$). The results show that in the ethanol solution, the correlations between water molecules are strongest, and the correlations between the hydroxyl groups in ethanol are weakest. The position of the first peak in $g_{OO}(r)$ is always around 2.7–2.8 Å, while the first minimum is more clearly pronounced when ethanol is involved. A qualitative comparison between these results, and those for $x_2 = 0.2$ in Figure 3 of Ref. [44], shows that the basic features are very similar. Fig. 5(b) shows the oxygen-hydroxyl hydrogen RDFs [$g_{OH}(r)$] for the same two liquids. The position of the first peak signals the O···H hydrogen bond, and it does not depend strongly on composition, being in the range 1.7–1.8 Å. The non-bonded coordination numbers (CNs) of oxygen atoms, and the associated cut-off distances r_{cut}, are shown in Table 4. r_{cut} was taken to be the position of the minimum between the first and second peaks in the RDF. The results show that the water oxygens are surrounded by slightly fewer oxygens

Table 4
Non-bonded coordination numbers (CNs), and associated cut-off distances, around oxygen atoms in water (OW) and in ethanol (OE). HW and HE denote the hydroxyl hydrogens in water and ethanol, respectively. Results are shown for pure water (0% ABV) and 40% ABV ethanol solution at $P = 1$ atm and $T = 298.15$ K. The fraction of atoms of a given type is indicated after the CN; for example, of the 4.17 oxygen atoms surrounding an OW atom in the ethanol solution, the fraction of other OWs is 0.884, and the fraction of OEs is 0.116.

ABV (%)	atom 1	atom 2	r_{cut} (Å)	CN (fraction)
0	OW	OW	3.31	4.43 (1.000)
40	OW	OW	3.34	3.69 (0.884)
40	OW	OE	3.35	0.48 (0.116)
40	OE	OW	3.35	2.48 (0.890)
40	OE	OE	3.36	0.31 (0.110)
0	OW	HW	2.40	1.83 (1.000)
40	OW	HW	2.40	1.59 (0.910)
40	OW	HE	2.46	0.16 (0.090)
40	OE	HW	2.46	1.42 (0.909)
40	OE	HE	2.53	0.14 (0.091)

and hydrogens in ethanol solution than in pure water, which correlates with the lower polarity of the solution. The fraction of ethanol oxygens in the first coordination shell of a given oxygen atom is slightly less than the overall mole fraction x_2. The fraction of ethanol hydroxyl hydrogens in the first coordination shell of a given oxygen atom is very similar to the overall mole fraction, equal to 0.0890.

3.2. Solutions with flavour molecules

In all of the results presented in this section, the ABVs are the nominal ones for the liquid layers, as shown in Table 2. The effective ABV is lower than the nominal one, and the values corrected for the surface excess of ethanol are given in Table 3. Since the bulk and surface concentrations of flavour molecules are low, the effective ABV should provide a reasonable estimate of the true alcoholic strength of the bulk product, and these are used in Section 4 for a discussion of the experimental relevance of the results.

3.2.1. Octane

Mass-density profiles for water, ethanol, and octane at 40% ABV are shown in Fig. 6. The water and ethanol profiles are hardly affected by the presence of a small number of octane molecules, which are strongly localised at the liquid-vapour interfaces. Octane is, of course, highly hydrophobic and immiscible with water; the solubility is 0.66 mg L^{-1} [45], and so the expected average number of octane molecules in the simulated pure-water layer is $\sim 10^{-3}$.

Since these molecules are at such low concentrations, in what follows, the probability density $p(z)$ is presented instead of $\rho(z)$; this is the probability density of finding at position z any atoms belonging to octane. Since the water and ethanol concentration profiles are hardly affected by the low concentrations of the flavour molecules, these will not be shown, but it will be obvious in each case where the liquid-vapour interfaces are positioned. Fig. 7(a) shows the probability densities for atoms in octane at all values of ABV. The distributions are not symmetric about $z = 0$ because the molecules are localised randomly at one of the two interfaces, and the concentration of molecules is low enough that they do not influence each other. Nonetheless, as the ethanol content is increased, the widths of the peaks at the liquid-vapour interfaces increase. In pure ethanol, there is an appreciable concentration of octane within the liquid layer, but there are still distinct peaks at the liquid-vapour interfaces. Note that octane is miscible in pure (bulk) ethanol [46].

3.2.2. Octanol

Fig. 7(b) shows the probability densities for atoms in octanol at all values of ABV. In water-rich solutions, the octanol is localised at the liquid-vapour interfaces. It starts to dissolve in the liquid layer at 50%

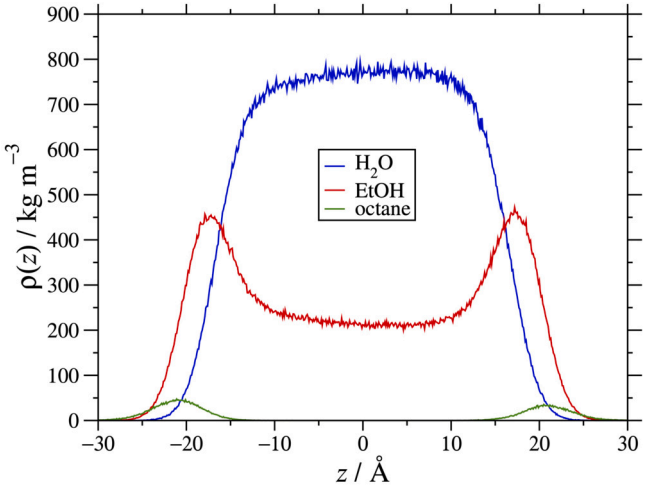

Fig. 6. Mass-density profiles for water, ethanol, and octane in a liquid layer with 40% ABV (nominal).

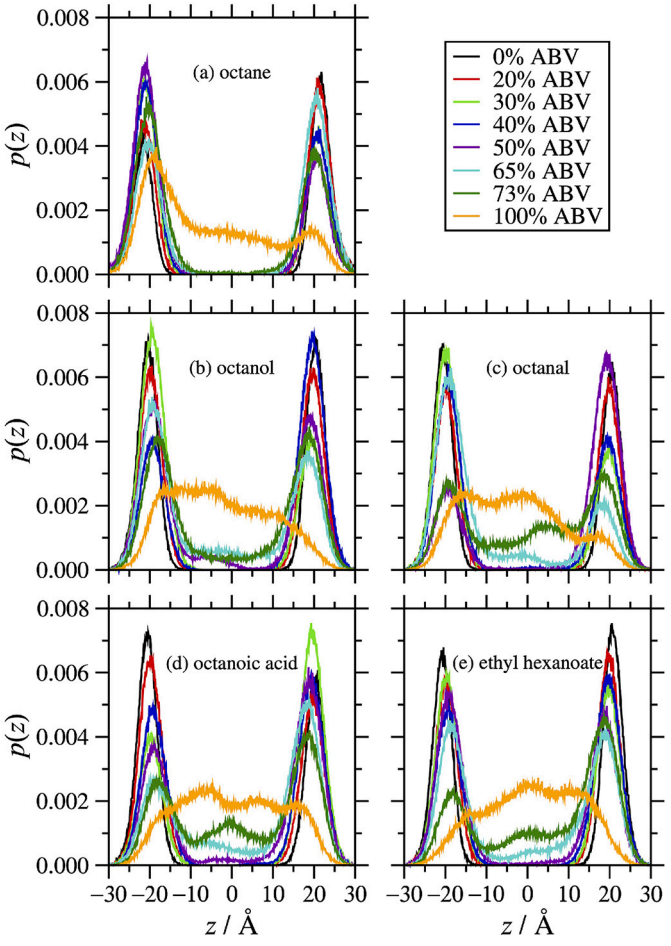

Fig. 7. Probability densities for atoms of flavour molecules in liquid layers with different values of nominal ABV: (a) octane; (b) octanol; (c) octanal; (d) octanoic acid; (e) ethyl hexanoate. The lines are coloured according to nominal ABV: 0% – black; 20% – red; 30% – light green; 40% – dark blue; 50% – purple; 65% – light blue; 73% – dark green; 100% – gold.

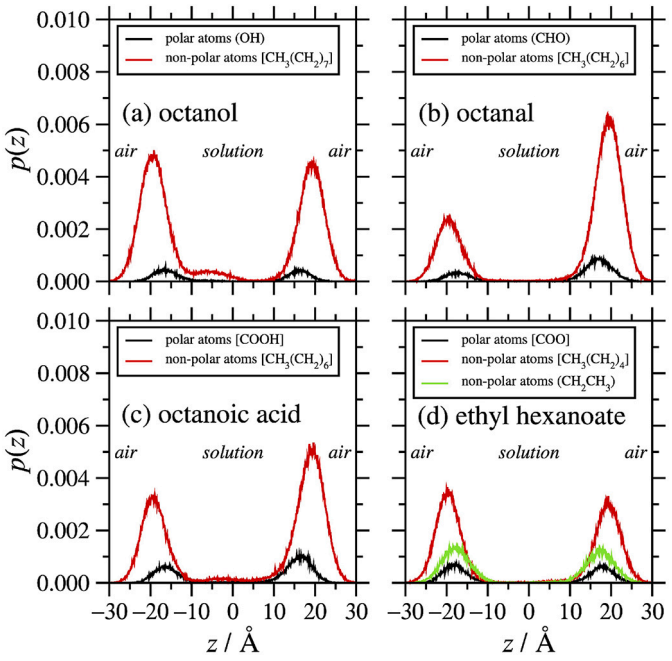

Fig. 8. Probability densities for polar and non-polar atoms of flavour molecules in liquid layers with 50% ABV (nominal): (a) octanol; (b) octanal; (c) octanoic acid; (d) ethyl hexanoate. The black lines are for the polar atoms, and the red and green lines are for the non-polar atoms.

ABV, but there are still distinct peaks at the liquid-vapour interfaces. At 100% ABV, the interfacial peaks are absent, and so the octanol is fully dissolved in the liquid layer.

To get insight on the orientations of the octanol molecules at the liquid-vapour interfaces, Fig. 8(a) shows individual probability densities for the non-polar atoms [$CH_3(CH_2)_7$] and polar atoms (OH) on the molecules, for the case of 50% ABV. These profiles show that the polar atoms are mainly on the liquid side of the interface, and the non-polar atoms are on the vapour side. There is a very small probability of the octanol molecules being found in the liquid layer.

3.2.3. Solutions with octanal

Fig. 7(c) shows the probability densities for atoms in octanal at all values of ABV. The results show that octanal begins to dissolve in the liquid at 65% ABV, and is fully soluble at 100% ABV. The probability densities for the non-polar atoms [$CH_3(CH_2)_6$] and polar (CHO) atoms at 50% ABV, shown in Fig. 8(b), indicate that the molecules orient themselves at the liquid-vapour interface similar to octanol molecules, with the polar heads in the liquid, and the non-polar tails pointing toward the vapour. As noted above, the asymmetry in the profiles is due to molecules being localised at one or other interface, at random.

3.2.4. Solutions with octanoic acid

Fig. 7(d) shows the probability densities for atoms in octanoic acid at all values of ABV. Below 50% ABV, the octanoic acid is strongly localised at the liquid-vapour interfaces. It begins to dissolve at 50% ABV, and at 100%, the interfacial peaks are absent, indicating complete dissolution. Fig. 8(c) shows that the non-polar atoms [$CH_3(CH_2)_6$] are on the vapour side of the interface, and the polar atoms (COOH) are on the liquid side, in a solution at 50% ABV. There is a very small probability of the octanoic acid molecules being found in the liquid layer.

3.2.5. Solutions with ethyl hexanoate

Fig. 7(e) shows the probability densities for atoms in ethyl hexanoate at all values of ABV. The results show that it begins to dissolve at 65% ABV, and is fully dissolved by 100% ABV. Fig. 8(d) shows that at 50% ABV, the non-polar $CH_3(CH_2)_4$ atoms are on the vapour side of the interface, and the non-polar CH_2CH_3 and polar COO atoms are on the liquid side.

4. Relevance to whisky tasting

4.1. Density profiles of water and ethanol

The density profiles presented in Fig. 3 reveal that water is distributed evenly in the bulk of the solution at all simulated ABV values. In contrast, ethanol exhibits a preference for the liquid-vapour interface in all solutions that contain any water. Essentially, ethanol acts like a surfactant [15], and accordingly leads to a decrease in the liquid-vapour interfacial tension, as shown in Fig. 4(b). Although the bulk-solution structure is not the focus of this study, it should be noted that simple alcohols like methanol and ethanol also exhibit mesoscopic clustering in water driven by the hydrophobic association of the non-polar moieties [47,48]. This is consistent with the observation that the polar moieties of solute molecules prefer the bulk of the solution, while the apolar moieties are localised at the interface (as shown in Fig. 8).

4.2. Concentration profiles of flavour molecules at different ABV

The high alcohol content of a spirit stabilises the product by retaining flavour molecules over a prolonged period. However, for the tasting experience to be possible, such molecules need to interact with the olfactory epithelium in the nasal cavity, or the taste buds on the tongue. Taste perception requires that the relevant molecules are present at the interface between the liquid and the human tissue, while aroma perception requires volatile molecules to be present at the liquid-vapour interface so that they can evaporate. In both cases, a compound that is mostly located in the bulk of the solution is unlikely to interact with the taste and aroma receptors, and therefore will not cause a flavour response. Similarly, a molecule that is concentrated at the interface is more likely to evaporate before the spirit can reach the mouth, resulting in a flavour response that will be mostly perceived on the nose. The density profiles presented in Section 3.2 are discussed below in terms of the probability of finding a given molecule at the interface and in the bulk of the solution at different alcohol strengths. To summarise those results, octane is strongly localised at the liquid-vapour interface in all but pure-ethanol solutions. Roughly speaking, octanol and octanoic acid begin to dissolve in solutions with 50% nominal ABV (41% effective ABV), while octanal and ethyl hexanoate begin to dissolve at 65% nominal ABV (59% effective ABV). Both octanol and octanoic acid have exposed groups of polar atoms, while the heteroatoms of octanal and ethyl hexanoate are separated and/or surrounded by carbon atoms, which may explain the observations. To make connections with real products, the effective ABVs from Table 3 are used below.

4.2.1. Solutions with octane

Octane is not generated during Scotch whisky production, and is not flavour active. The reason for including octane in this study was that its hydrophobicity is higher than that of the other molecules, while having a similar molecular structure and mass. It is therefore a model of a highly hydrophobic molecule, and it provides a reference point for the other flavour molecules. The simulations show that octane is only found inside the solution at 100% ABV (pure ethanol), and even in this case, it still exhibits a preference for the interface. A molecule with the hydrophobicity of octane may be present in the initial distillate, but would likely be lost when the spirit is diluted to cask strength. Any remaining traces of such a compound would be concentrated at the liquid-vapour interface and could potentially have an aroma impact if present at high enough levels.

4.2.2. Solutions with octanol

Octanol is associated with a waxy aroma in Scotch whisky. The simulations show that octanol is essentially concentrated at the liquid-

vapour interface at all alcoholic strengths below 41% ABV. This range includes the common strengths of sensory testing, and regular bottle strength products. In such products, octanol will easily evaporate and cause a sensory response through stimulation of the olfactory system. At higher strengths, octanol is still mostly concentrated at the interface, with a smaller proportion located in the bulk of the solution. In those cases, octanol may still be detected, but at a lower intensity. Finally, an octanol solution in pure ethanol would have most of the solute located in the bulk of the solution where it would be unlikely to initiate a flavour response.

4.2.3. Solutions with octanal

Octanal has a soapy or oily aroma. At alcoholic strengths of 41% ABV or lower, octanal is mainly located at the liquid-vapour interface, suggesting that in bottle strength products, octanal will mostly cause an olfactory response. In cask strength products (59%, 68% ABV), octanal partly dissolves into the bulk of the solution, while still showing preference for the interface, indicating that it will still be detectable by the olfactory system, albeit at a lower intensity. In pure ethanol (100% ABV), octanal is mostly located in the bulk of the solution, indicating that no flavour response is likely to be triggered.

4.2.4. Solutions with octanoic acid

Octanoic acid has a goaty aroma, reminiscent of goat's cheese, and sour taste. At strengths of 29% and below, octanoic acid is primarily located at the liquid-vapour interface, and will therefore be likely to induce a sensory response (aroma and taste). In products bottled at 41% ABV, octanoic acid will be partly located in the bulk of the solution, suggesting implications for both taste and aroma. At 59% or 68% ABV, a more significant part of the solute is located in the bulk, but it still exhibits a preference for the interface, which again promises a response involving both taste and aroma. Once more, octanoic acid in pure ethanol is unlikely to produce a sensory response, being mostly located in the bulk solution.

4.2.5. Solutions with ethyl hexanoate

Ethyl hexanoate is associated with fruity aromas in Scotch whisky. Its flavour properties at different alcohol strengths will be similar to those of octanoic acid: in bottle strength products (41% ABV) and those with a lower ABV, ethyl hexanoate will most likely produce a purely olfactory response. In cask strength products (59%, 68% ABV), a response is still likely to occur, though again this may be at reduced intensity.

5. Conclusions

In this work, MD simulations were performed to explore the behaviour of a series of flavour molecules relevant to the whisky industry at the liquid-vapour interface of solutions with various values of ABV. Octanol, octanal, octanoic acid, and ethyl hexanoate were selected due to their varying flavour properties and degrees of hydrophobicity, while octane (which is not present in whisky and not flavour active) was selected as a model of a hydrophobic compound. An additional study of pure solutions of ethanol/water was conducted to analyse the surface excess of ethanol at the chosen simulation conditions. The role of the simulation work is to provide atomistic details on the underlying behaviour of the systems. It was observed that the surface excess of ethanol is significant compared to the content of the bulk solution, and so it has to be taken into account when trying to simulate a layer with a given ABV. Furthermore, it was shown that the results from MD simulations compare favourably with experimental values of the ethanol surface excess, and the interfacial tension, of ethanol/water solutions.

In the systems with flavour molecules, it was shown how decreasing the ABV can lead to an increase in surface concentration of these compounds, such as might happen when adding water to a cask-strength dram of whisky. The level of surface activity depends on the hydrophobicity of the flavour molecules, with octane being surface active at much higher values of ABV than the other molecules, and octanol and octanoic acid being active at lower ABVs than the others. Furthermore, it was shown how molecules with hydrophobic and hydrophilic moieties have surfactant-like behaviour at the liquid-vapour interface, showing preferential orientation of the polar moieties towards the inside of the liquid layer. Overall, this study shows how MD simulations can help in understanding the complex behaviours of flavour molecules in ethanol/water solutions, and complement available experimental techniques. A particular advantage of MD simulations is that high-throughput screening could be used to gain an improved understanding of the links between composition and sensory perception. Further exploration of alcohol strength impacts could also provide useful information for the development of low-alcohol beverages that simulate the tasting experience of regular strength spirits.

CRediT authorship contribution statement

E.E.S.: Validation, Formal analysis, Investigation, Data curation, Writing – reviewing and editing, Visualisation. **R.F.G.A.**: Conceptualisation, Methodology, Software, Validation, Formal analysis, Investigation, Data curation, Writing – original draft preparation, Writing – reviewing and editing, Visualisation, Supervision. **P.J.C.**: Conceptualisation, Methodology, Formal analysis, Resources, Writing – original draft preparation, Writing – reviewing and editing, Supervision, Project administration, Funding acquisition. **J.M.C.**: Writing – review and editing. **B.H.**: Writing – review and editing. **F.J.**: Writing – review and editing. **J.C.-N.**: Conceptualisation, Methodology, Writing – original draft preparation, Writing – review and editing, Visualisation, Project administration.

Declaration of competing interest

The authors declare that they have no known competing financial interests or personal relationships that could have appeared to influence the work reported in this paper.

Data availability

Data will be made available on request.

Acknowledgements

The authors are honoured to contribute to this Virtual Special Issue marking the 80th birthday of Professor Myroslav Holovko – an outstanding scientist and a true gentleman.

The work of E.E.S. was carried out as part of an undergraduate research project, supported by the School of Chemistry at the University of Edinburgh. The authors thank the Nvidia Corporation for the donation of Titan Xp and Titan V GPUs used in the research.

References

[1] R. Aylott, Chapter 19 – Whisky analysis, in: I. Russell, G.G. Stewart, J. Kellershohn (Eds.), Whisky and Other Spirits, third edition, Academic Press, 2022, pp. 335–362.
[2] T.A. Bringhurst, B.M. Harrison, J. Brosnan, Chapter 10 – Scotch whisky: raw material selection and processing, in: I. Russell, G.G. Stewart, J. Kellershohn (Eds.), Whisky and Other Spirits, third edition, Academic Press, 2022, pp. 137–203.
[3] I. Russell, G.G. Stewart, Chapter 12 – Distilling yeast and fermentation, in: I. Russell, G.G. Stewart, J. Kellershohn (Eds.), Whisky and Other Spirits, third edition, Academic Press, 2022, pp. 213–236.
[4] N.R. Wilson, Chapter 13 – Contamination: bacteria and wild yeasts in whisky fermentation, in: I. Russell, G.G. Stewart, J. Kellershohn (Eds.), Whisky and Other Spirits, third edition, Academic Press, 2022, pp. 237–245.
[5] J. Conner, Chapter 16 – Maturation, in: I. Russell, G.G. Stewart, J. Kellershohn (Eds.), Whisky and Other Spirits, third edition, Academic Press, 2022, pp. 291–311.
[6] The Scotch Whisky Regulations 2009, UK Statutory Instrument No. 2890 (26 October 2009), https://www.legislation.gov.uk/uksi/2009/2890/contents/made.
[7] F. Jack, Chapter 18 – Sensory analysis, in: I. Russell, G.G. Stewart, J. Kellershohn (Eds.), Whisky and Other Spirits, third edition, Academic Press, 2022, pp. 321–333.

[8] E.H.B. Maia, L.C. Assis, T.A. de Oliveira, A.M. da Silva, A.G. Taranto, Structure-based virtual screening: from classical to artificial intelligence, Front. Chem. 8 (2020) 343.
[9] J. Lyu, S. Wang, T.E. Balius, I. Singh, A. Levit, Y.S. Moroz, M.J. O'Meara, T. Che, E. Algaa, K. Tolmachova, A.A. Tolmachev, B.K. Shoichet, B.L. Roth, J.J. Irwin, Ultra-large library docking for discovering new chemotypes, Nature 566 (2019) 224–229.
[10] C. Gorgulla, A. Boeszoermenyi, Z.F. Wang, P.D. Fischer, P.W. Coote, D. Padmanabha, M. Krishna, Y.S. Malets, D.S. Radchenko, Y.S. Moroz, D.A. Scott, K. Fackeldey, M. Hoffmann, I. Iavniuk, G. Wagner, H. Arthanari, An open-source drug discovery platform enables ultra-large virtual screens, Nature 580 (2020) 663–668.
[11] R.F.G. Apóstolo, G. Tsagkaropoulou, P.J. Camp, Molecular adsorption, self-assembly, and friction in lubricants, J. Mol. Liq. 277 (2019) 606–612.
[12] M. Lbadaoui-Darvas, G. Garberoglio, K.S. Karadima, M.N.D.S. Cordeiro, A. Nenes, S. Takahama, Molecular simulations of interfacial systems: challenges, applications and future perspectives, Mol. Simul. (2021), https://doi.org/10.1080/08927022.2021.1980215.
[13] J. Du, J. Dong, S. Du, K. Zhang, J. Yu, S. Hu, H. Yin, Understanding thermostability factors of barley limit dextrinase by molecular dynamics simulations, Front. Mol. Biosci. 7 (2020) 51.
[14] J. Du, S. Hua, J. Dong, R. Wu, J. Yua, H. Yin, Exploring the factors that affect the themostability of barley limit dextrinase – inhibitor complex, J. Mol. Graph. Model. 109 (2021) 108043.
[15] B.C.G. Karlsson, R. Friedman, Dilution of whisky – the molecular perspective, Sci. Rep. 7 (2017) 6489.
[16] LAMMPS Molecular Dynamics Simulator, https://www.lammps.org, 2021.
[17] S. Plimpton, Fast parallel algorithms for short-range molecular dynamics, J. Comput. Phys. 117 (1995) 1–19.
[18] A.P. Thompson, H.M. Aktulga, R. Berger, D.S. Bolintineanu, W.M. Brown, P.S. Crozier, P.J. in't Veld, A. Kohlmeyer, S.G. Moore, T.D. Nguyen, R. Shan, M.J. Stevens, J. Tranchida, C. Trott, S.J. Plimpton, LAMMPS – a flexible simulation tool for particle-based materials modeling at the atomic, meso, and continuum scales, Comput. Phys. Commun. 271 (2022) 108171.
[19] L. Martínez, R. Andrade, E.G. Birgin, J.M. Martínez, PACKMOL: a package for building initial configurations for molecular dynamics simulations, J. Comput. Chem. 30 (2009) 2157–2164.
[20] W. Humphrey, A. Dalke, K. Schulten, VMD – visual molecular dynamics, J. Mol. Graph. 14 (1996) 33–38.
[21] W.L. Jorgensen, J.D. Madura, C.J. Swenson, Optimized intermolecular potential functions for liquid hydrocarbons, J. Am. Chem. Soc. 106 (1984) 6638–6646.
[22] W.L. Jorgensen, J. Tirado-Rives, The OPLS potential functions for proteins. Energy minimizations for crystals of cyclic peptides and crambin, J. Am. Chem. Soc. 110 (1988) 1657–1666.
[23] W.L. Jorgensen, D.S. Maxwell, J. Tirado-Rives, Development and testing of the OPLS all-atom force field on conformational energetics and properties of organic liquids, J. Am. Chem. Soc. 118 (1996) 11225–11236.
[24] W. Damm, A. Frontera, J. Tirado-Rives, W.L. Jorgensen, OPLS all-atom force field for carbohydrates, J. Comput. Chem. 18 (1997) 1955–1970.
[25] S.W.I. Siu, K. Pluhackova, R.A. Böckmann, Optimization of the OPLS-AA force field for long hydrocarbons, J. Chem. Theory Comput. 8 (2012) 1459–1470.
[26] W.L. Jorgensen, J. Chandrasekhar, J.D. Madura, R.W. Impey, M.L. Klein, Comparison of simple potential functions for simulating liquid water, J. Chem. Phys. 79 (1983) 926–935.
[27] R.J. Good, C.J. Hope, New combining rule for intermolecular distances in intermolecular potential functions, J. Chem. Phys. 53 (1970) 540–543.
[28] M.P. Allen, D.J. Tildesley, Computer Simulation of Liquids, 2nd edition, Oxford University Press, Oxford, 2016.
[29] J.-P.E. Grolier, E. Wilhelm, Excess volumes and excess heat capacities of water + ethanol at 298.15 K, Fluid Phase Equilib. 6 (1981) 283–287.
[30] J.S. Rowlinson, B. Widom, Molecular Theory of Capillarity, Dover Publications, Inc., Mineola, New York, 2002.
[31] W. Wagner, A. Pruß, The IAPWS formulation 1995 for the thermodynamic properties of ordinary water substance for general and scientific use, J. Phys. Chem. Ref. Data 31 (2002) 387–535.
[32] J.D. Weeks, Structure and thermodynamics of the liquid–vapor interface, J. Chem. Phys. 67 (1977) 3106–3121.
[33] C. Ormanoudis, C. Dakos, C. Panaylotou, Volumetric properties of binary mixtures. 2. Mixtures of n-hexane with ethanol and 1-propanol, J. Chem. Eng. Data 36 (1991) 39–42.
[34] Z.X. Li, J.R. Lu, D.A. Styrkas, R.K. Thomas, A.R. Rennie, J. Penfold, The structure of the surface of ethanol/water mixtures, Mol. Phys. 80 (1993) 925–939.
[35] Y.F. Yano, Correlation between surface and bulk structures of alcohol-water mixtures, J. Colloid Interface Sci. 284 (2005) 255–259.
[36] G. Vázquez, E. Alvarez, J.M. Navaza, Surface tension of alcohol + water from 20 to 50 °C, J. Chem. Eng. Data 40 (1995) 611–614.
[37] R. Strey, Y. Viisanen, M. Aratono, J.P. Kratohvil, Q. Yin, S.E. Friberg, On the necessity of using activities in the Gibbs equation, J. Phys. Chem. B 103 (1999) 9112–9116.
[38] I.S. Khattab, F. Bandarkar, M.A.A. Fakhree, A. Jouyban, Density, viscosity, and surface tension of water+ethanol mixtures from 293 to 323 K, Korean J. Chem. Eng. 29 (2012) 812–817.
[39] C. Vega, E. de Miguel, Surface tension of the most popular models of water by using the test-area simulation method, J. Chem. Phys. 126 (2007) 154707.
[40] L. Pusztai, O. Pizio, S. Sokolowski, Comparison of interaction potentials of liquid water with respect to their consistency with neutron diffraction data of pure heavy water, J. Chem. Phys. 129 (2008) 184103.
[41] P.T. Kiss, A. Baranyai, Sources of the deficiencies in the popular SPC/E and TIP3P models of water, J. Chem. Phys. 134 (2011) 054106.
[42] Z. Steinczinger, P. Jóvári, L. Pusztai, Comparison of 9 classical interaction potentials of liquid water: simultaneous Reverse Monte Carlo modeling of X-ray and neutron diffraction results and partial radial distribution functions from computer simulations, J. Mol. Liq. 228 (2017) 19–24.
[43] S.P. Kadaoluwa Pathirannahalage, N. Meftahi, A. Elbourne, A.C.G. Weiss, C.F. McConville, A. Padua, D.A. Winkler, M. Costa Gomes, T.L. Greaves, T.C. Le, Q.A. Besford, A.J. Christofferson, Systematic comparison of the structural and dynamic properties of commonly used water models for molecular dynamics simulations, J. Chem. Inf. Model. 61 (2021) 4521–4536.
[44] O. Gereben, L. Pusztai, Investigation of the structure of ethanol–water mixtures by molecular dynamics simulation I: analyses concerning the hydrogen-bonded pairs, J. Phys. Chem. B 119 (2015) 3070–3084.
[45] S.H. Yalkowsky, Y. He, P. Jain, Handbook of Aqueous Solubility Data, 2nd edition, CRC Press, Boca Raton, FL, 2010.
[46] J. Rumble, CRC Handbook of Chemistry and Physics, 103rd edition, CRC Press, Boca Raton, FL, 2022.
[47] S. Dixit, J. Crain, W.C.K. Poon, J.L. Finney, A.K. Soper, Molecular segregation observed in a concentrated alcohol-water solution, Nature 416 (2002) 829–832.
[48] R. Li, C. D'Agostino, J. McGregor, M.D. Mantle, J.A. Zeitler, L.F. Gladden, Mesoscopic structuring and dynamics of alcohol/water solutions probed by terahertz time-domain spectroscopy and pulsed field gradient nuclear magnetic resonance, J. Phys. Chem. B 118 (2014) 10156–10166.